Proceedings of the ASME 2019
International Design Engineering Technical Conferences
and Computers and Information in Engineering Conference
IDETC/CIE2019
August 18-21, 2019, Anaheim, CA, USA

DETC2019-98354

ON THE FRICTION ISOLATOR FOR PRECISION MOTION CONTROL AND ITS DYNAMICS

Xin Dong, Chinedum Okwudire
Department of Mechanical Engineering
University of Michigan, Ann Arbor, MI, USA

Jiamin Wang, Oumar Barry[1]
Department of Mechanical Engineering
Virginia Tech, Blacksburg, VA, USA

ABSTRACT

Motion stages are widely used for precision positioning in manufacturing and metrology applications. However, they suffer from nonlinear pre-motion (i.e., "static") friction which adversely affects their precision and motion speed. Existing friction compensation methods are not robust enough to handle the highly nonlinear and variable dynamic behavior of pre-motion friction. Therefore, the first two authors have proposed the concept of a friction isolator as a simple and robust solution to mitigate the undesirable effects of pre-motion friction in precision motion stages. They experimentally demonstrated that a motion stage with friction isolator can achieve significantly improved precision, speed and robustness to variations in pre-motion friction. However, a theoretical study was not carried out to fundamentally understand the dynamic phenomena associated with using a friction isolator on a motion stage. This introductory paper investigates the dynamics of a PD-controlled motion stage with friction isolator. The influence of the friction isolator on the response and stability of the system is examined through theoretical and numerical analysis. It is shown, using a case study, that the addition of a friction isolator shrinks the range of P and D gains that can stabilize the motion stage. Several other case studies that include the effects of external excitation and integral controller are carried out to motivate deeper dynamic analyses of the friction isolator for precision motion control.

Keywords: Friction-induced vibration, Friction oscillator, LuGre model, Stability

1. BACKGROUND AND INTRODUCTION

Motion stages are used for precision positioning in a wide range of manufacturing and metrology-related processes, such as machining, additive manufacturing and semi-conductor fabrication. Mechanical bearings (i.e., sliding, and, especially rolling bearings) are commonly used in these precision motion stages due to their large motion range, high axis stiffness and cost-effectiveness [1]. However, mechanical bearings experience nonlinear pre-motion (i.e., "static") friction arising from their inherent rolling elements, end seals and wipers [2]. In pre-motion regime, friction behaves as a highly nonlinear hysteretic spring due to adhesive forces from asperities on the contacting surfaces [2][3].

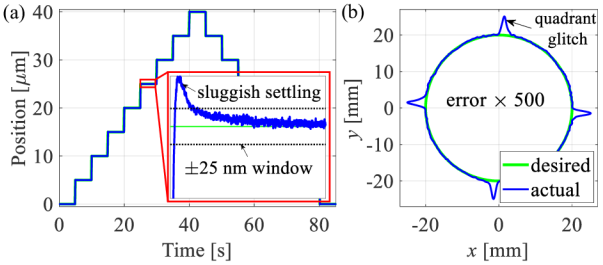

FIGURE 1: (A) POINT-TO-POINT POSITIONING MOVES AND (B) CIRCLE TESTS USING A CONVENTIONAL MOTION STAGE.

Conventional servo controllers (e.g., PID, P/PI, etc.), which are widely used in practice, often encounter difficulties when trying to overcome the highly nonlinear and variable stiffness of pre-motion friction, causing severely diminished performance such as large tracking errors, long settling times and stick-slip phenomena [4]-[7]. For example, during point-to-point positioning, as shown in Fig. 1 (a), the stage is commanded to travel to and settle within a pre-specified vicinity (i.e., window) of a target position as fast as possible. Pre-motion friction dominates as the stage gets within micrometers of its target position, leading to very sluggish settling performance [4][7][8]. Similarly, during tracking applications, where the stage is commanded to follow a given trajectory (e.g., circular tracking or triangular scanning), large position errors (i.e., glitches) often occur as the servo controller tries to overcome pre-motion friction at motion reversals – see Fig. 1 (b) [9].

Compensation methods are often used to mitigate the undesirable effects of pre-motion friction, including high-gain feedback [5], model-based feedforward and feedback controllers

[1] Contact author: obarry@vt.edu

[9]. However, high-gain controllers could easily lead to large overshoot and limit cycles, and model-based compensation methods often suffer from robustness and stability problems due to the rapid and nonlinear changes of pre-motion friction [6].

The friction isolator[2] (FI). – also known as the compliant joint method – has recently been proposed as an effective and robust method for mitigating pre-motion friction [9][10]. The idea is to connect the mechanical bearing to the moving table of a motion stage using a joint that is very compliant in the motion direction, thus effectively isolating the motion stage from strong nonlinearities associated with pre-motion friction. As is briefly shown in Section 2, the FI enables superior performance and robustness of friction compensation methods, leading to significantly reduced motion error and settling time in tracking and point-to-point positioning applications, respectively [9][10].

However, the introduction of a FI to a motion stage leads to nonlinear interactions between friction, servo controller and FI dynamics. These interactions can be linked to friction-induced oscillation, which is a well-studied topic in nonlinear dynamics. The key contributions of this paper are, therefore, to:

1) In Section 3, review relevant works on friction-induced oscillation and highlight ways in which they do not address the dynamics of a servo-controlled motion stage with FI;
2) In Section 4, use theoretical and numerical analyses carried out on a model of a servo-controlled stage with FI to demonstrate interesting phenomena associated with it;
3) In Section 5, discuss other interesting features of a servo-controlled stage equipped with FI to motivate further study of it by the nonlinear dynamics community.

This is followed by conclusions and future work in Section 6.

2. FRICTION ISOLATOR FOR MITIGATING PRE-MOTION FRICTION

2.1. Concept

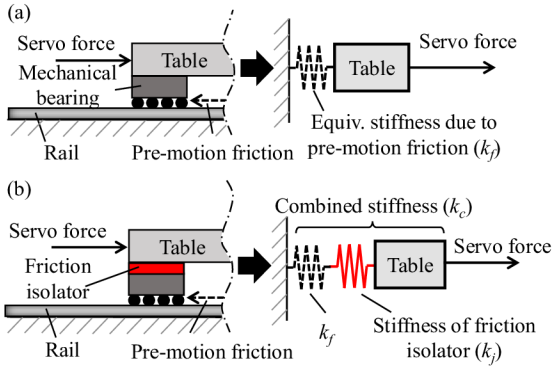

FIGURE 2: SCHEMATICS OF A PRECISION MOTION STAGE WITH MECHANICAL BEARING ATTACHED TO THE TABLE (A) RIGIDLY AND (B) USING FI.

Fig. 2 (a) illustrates a conventional precision motion stage equipped with a mechanical bearing that is rigidly attached to the moving table. As is common practice, pre-motion friction is modeled as an equivalent spring of nonlinear stiffness k_f connecting the table to ground [2]. At the start of motion or motion reversals, k_f is very large; but as more servo force is applied to counteract friction, k_f rapidly reduces and eventually becomes zero, allowing gross motion of the stage. The highly nonlinear dynamics of pre-motion friction causes large position errors and sluggish settling behavior because the servo errors accumulate as the controller tries to overcome large value of k_f when starting from rest (or after motion reversals).

Fig. 2 (b) shows the concept of the friction isolator (FI) for mitigating undesirable effects of pre-motion friction in precision motion stage, as presented in prior works by the first two authors (and their collaborators) [9][10]. Rather than being rigidly attached to the moving table of the stage, the mechanical bearing is attached using a joint of stiffness k_j in the motion direction. Accordingly, the stage with FI can be modeled, *statically*, as a series combination of k_f and k_j, with combined stiffness $k_c = k_f k_j/(k_f + k_j)$. Note that the bearing mass and damping of FI are intentionally ignored here, for the sake of simplicity; they are considered starting from Section 3. Using the simple static model, the sensitivity of the combined stiffness k_c to variations in k_f is given by

$$\frac{\partial k_c}{\partial k_f} = \left(\frac{\psi}{1+\psi}\right)^2; \text{ where } \psi = \frac{k_j}{k_f} \quad (1)$$

Note that if $k_j << k_f$, $\psi \to 0$ and the sensitivity of k_c to errors in k_f becomes very small. In other words, a very small k_j dominates the combined stiffness felt by the servo controller when k_f is very large in the pre-motion regime, that is, $k_c \to k_j$ even when $k_f \to \infty$. Therefore, if $k_j << k_f$ and k_j is precisely known, accurate model-based compensation of pre-motion friction can be achieved even when a significant amount of error exists in k_f (due to low-fidelity friction modeling or variations of friction).

2.2. Experimental Validation

Model-based feedforward (FF) compensation of pre-motion friction is carried out on a motion stage with and without FI, whose design is presented in [9]. A popular pre-motion friction model is implemented in the FF compensator, namely the Dahl model [5]. Details about the friction model and parameter identification are described in [9]. Circular motions with 20 mm radius and tangential velocities ranging from 6 mm/s to 125 mm/s are used as reference commands to the precision motion stage. Since it is a single-axis stage, x-axis reference trajectories for the circular motions are utilized to test the following cases:

- Baseline: motion stage without FI nor FF compensation;
- FF w/o FI: FF compensation on the stage without FI;
- FF w/ FI; FF compensation on the stage with FI.

The robustness of FF compensation in the presence of model parameter errors due to changing frictional stiffness is tested by introducing deviations of 0, ±10, ±20 and ±50% into the identified frictional stiffness (k_f). Fig. 3 (a) shows the mean

[2] The term "friction isolator" is, on rare occasions, used as shorthand for "friction-pendulum isolator" in the literature, e.g., [11]. However, the friction-pendulum isolator is a vibration isolator that uses Coulomb friction for damping, not a device that isolates a system from deleterious effects of friction, as is the case with the friction isolator discussed here.

percentage reductions of peak errors (relative to the baseline case) together with the corresponding $\pm 1\sigma$ (standard deviation) bands based on all deviation cases. The peak errors correspond to the quadrant glitches shown in Fig. 1 (b). It is observed that the FF w/o FI case performs even worse than the baseline case for low velocity circular tests, due to its low accuracy [9]. Amazingly, the FF w/ FI case achieves significantly better level of performance than the case without FI. Moreover, FF w/o FI case suffers from large performance variations due to the errors in their pre-motion frictional parameters. However, the FF w/ FI case provides very accurate and robust tracking performance because of its reduced sensitivity to errors in pre-motion frictional stiffness brought about by the proposed FI. FF compensations with other more advanced friction models have been tested in which the FF w/ FI case demonstrated superior performance as well [9]. Similar experiments have also been performed for several other circle radiuses (namely, 5 mm, 500 μm, 50 μm and 5 μm) and speeds. The results, which are reported in [12], show similar excellent performance of FI in terms of the accuracy and robustness.

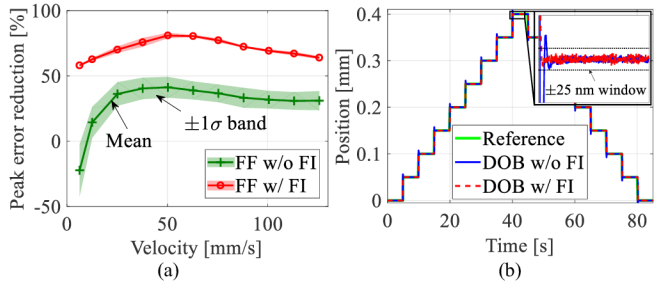

FIGURE 3: (A) PEAK ERRORS DURING CIRCLE TESTS AND (B) SETTLING TIMES DURING 50 μm P2P MOTIONS.

Experiments are also carried out to test the settling performance of the stage with and without FI during point-to-point (P2P) positioning motions; note that a disturbance observer (DOB) is implemented in both cases as an example of model-based feedback friction compensation. Fig. 3 (b) shows the results from the P2P staircase commands with the 50 μm steps. The stage with FI settles much faster than the stage without it for all steps of the 50 μm cases, achieving 72% reduction in mean settling time. The same experiments are repeated with various step sizes, ranging from 50 nm to 5 mm, and similar benefits of FI are observed [10]. Moreover, the stage with FI is also shown to be much more robust to variations in friction compared to the conventional precision motion stage, as reported in [10]. Given the remarkable improvements in positioning precision and speed brought by the FI, it is of interest to understand beneficial and harmful effects of its dynamics on precision motion stages.

3. REVIEW OF RELATED LITERATURE

Fig. 4 (a) shows a rudimentary dynamic model of a servo-controlled motion stage with FI. The moving table of mass m_t is connected to the ground by stiffness k and damping c, which respectively represent the proportional (P) and derivative (D) gains of the servo controller regulating the table's position (i.e., x). Force f_{servo} is added to account for any additional servo forces that may be applied to the table (e.g., integral action). The FI is modeled as a mass m_b connected to m_t via stiffness k_j and c_j; note that mass m_b accounts for the combined mass of the FI and mechanical bearing attached to it, whose position is defined by x_b. Friction force f_f is applied to m_b via a moving platform whose motion is prescribed by x_p.

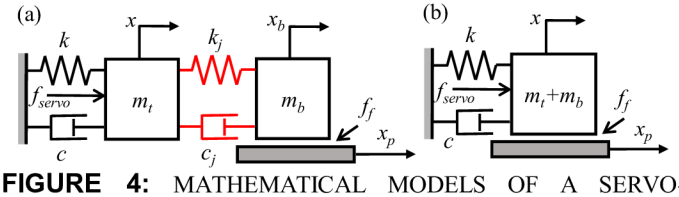

FIGURE 4: MATHEMATICAL MODELS OF A SERVO-CONTROLLED STAGE (A) WITH AND (B) WITHOUT FI.

Fig. 4 (b) shows a servo-controlled stage without FI. Notice that the PD-controlled stage (i.e., $f_{servo} = 0$) without FI represents a one degree-of-freedom (DOF) friction oscillator, which has been studied extensively in the literature in the context of friction-induced vibration with self and/or external excitations [13][14]. Studies on friction oscillators have usually been performed using static friction models (e.g., dry friction). However, dynamic models that include the nonlinear stiffness characteristics of pre-motion friction have been adopted in some studies to capture the smooth transitions between stick and slip that are commonly observed in experiments [15].

The 1-DOF oscillator has also been extended to multiple DOF for investigating the effects of mode coupling or obtaining generalized characteristics of the system [15]-[17]. However, these multi-DOF models either include an orthogonal DOF or simply connect several oscillators in series, with friction acting on each oscillator. This is unlike the FI (e.g., Fig. 4 (a)) where friction only acts on the bearing (m_b) not on the main stage (m_t).

The closest work that adopts a similar configuration as that in Fig. 4 (a) is [17], in which a 2-DOF model is used to study the stick-slip characteristics of the friction oscillator with tangential contact compliance. However, a Coulomb model that only captures dry friction is used for analysis in [17]; the highly nonlinear behavior of pre-motion friction is ignored. Moreover, the model in [17], and those typically used in studying friction oscillators, does not include the effects of other important servo controllers that are widely implemented on precision motion stages, e.g., the integral controller. Therefore, the rest of this paper is intended as a first step in addressing the deficiencies of prior work on friction oscillators in the context of servo-controlled motion stages with one or more FIs.

4. DYNAMICS OF FRICTION ISOLATOR

In this section, the stability of a PD-controlled motion stage with FI is studied using analytical and numerical methods; LuGre model, [18] which includes the pre-motion frictional dynamics, is used in the analysis. It is observed in simulation that the addition of FI shrinks the range of P and D servo gains that can stabilize the motion stage. Theoretical analyses of linear stability around equilibrium support these numerical findings, which help highlight the dynamics of a servo-controlled motion stage with FI needs further study.

4.1. Modeling

For simplicity, it is assumed that the platform in Fig. 4 experiences constant velocity motion with zero initial displacement, i.e., $x_p(0) = 0$ and $\ddot{x}_p = 0$. The dynamics of the PD-controlled stage (i.e., $f_{servo} = 0$) with FI is then described by

$$\begin{aligned} &m_t\ddot{x} + c\dot{x} + kx + c_j(\dot{x} - \dot{x}_b) + k_j(x - x_b) = 0; \\ &m_b\ddot{x}_b + f_f + c_j(\dot{x}_b - \dot{x}) + k_j(x_b - x) = 0 \end{aligned} \tag{2}$$

Similarly, the dynamics of the PD-controlled motion stage without FI – see Fig 4 (b) – is given by

$$(m_t + m_b)\ddot{x} + f_f + c\dot{x} + kx = 0 \tag{3}$$

The friction force is calculated through the LuGre model [18] which captures the nonlinear stiffness characteristics of pre-motion friction. To realize this, the LuGre model introduces an internal state z that is used to represent the average deflection of the contact bristles between two surfaces at the friction interface. Its dynamics is given by

$$\dot{z} = v - \frac{|v|}{g(v)}z \tag{4}$$

where v is the relative velocity between two moving surfaces (i.e., $v = \dot{x}_b - \dot{x}_p$ and $v = \dot{x} - \dot{x}_p$ for the cases with and without FI) and $g(v)$ is parameterized to describe the Stribeck effect

$$\sigma_0 g(v) = f_C + (f_S - f_C)e^{-(v/v_S)^2} \tag{5}$$

where f_C is the Coulomb friction, f_S is the static friction, v_s is the Stribeck velocity threshold and σ_0 is the initial contact stiffness of the bristle (i.e., initial pre-motion frictional stiffness). The modeled friction force is then obtained as

$$f_f = \sigma_0 z + \sigma_1\dot{z} + \sigma_2 v \tag{6}$$

where σ_1 is the micro-damping of the bristle and σ_2 accounts for macroscopic viscous friction.

By settling $\dot{z} = 0$, equilibriums of the internal friction state z are obtained as

$$v = 0 \quad \text{or} \quad z = \text{sgn}(v)g(v) \tag{7}$$

The sticking equilibrium is obtained when $v = 0$, while the slipping equilibrium is obtained when $z = \text{sgn}(v)g(v)$. Note that the fix points of any dynamic system that involves LuGre friction model have to satisfy either of these two conditions. In some rare cases, the two equilibriums may overlap. Substituting Eqs. (4)-(6) into (3), the state equations of the PD-controlled stage without FI can be written as

$$\delta_1 = \begin{bmatrix} x \\ v \\ z \end{bmatrix}; \dot{\delta}_1 = \begin{bmatrix} v + \dot{x}_p \\ -\dfrac{c(v + \dot{x}_p) + kx + f_f}{m_t + m_b} \\ v - h(v)z \end{bmatrix}; \; h(v) = \frac{|v|}{g(v)} \tag{8}$$

where δ_1 contains the states of the system. Similarly, the state equations of the stage with FI can be written as

$$\begin{aligned} &\delta_2 = [x \quad \dot{x} \quad x_b \quad v \quad z]^T; \\ &\dot{\delta}_2 = \left[\dot{x} \quad -\frac{c\dot{x} + kx + f_l}{m_t} \quad v + \dot{x}_p \quad -\frac{f_f - f_l}{m_b} \quad v - h(v)z\right]^T \end{aligned} \tag{9}$$

where δ_2 is the state variable and f_l is defined as,

$$f_l = c_j(v + \dot{x}_p - \dot{x}) + k_j(x_b - x) \tag{10}$$

4.2. Numerical Simulation

The PD-controlled motion stage with and without FI is numerically simulated using state equations described in Eqs. (8) and (9). Note that parameters obtained from the motion stage are used in the simulation – see Table 1; details of LuGre model identification are discussed in the appendix.

TABLE 1: PARAMETERS USED FOR SIMULATION BASED ON MEASURED VALUES FROM THE MOTION STAGE.

m_t [kg]	1	f_S [N]	6.5
m_b [kg]	0.5	σ_0 [N/m]	2.2×10^6
k_j [N/m]	40,000	σ_1 [Ns/m]	237
c_j [Ns/m]	2	σ_2 [Ns/m]	14.2
f_C [N]	5.1	v_s [mm/s]	16.7

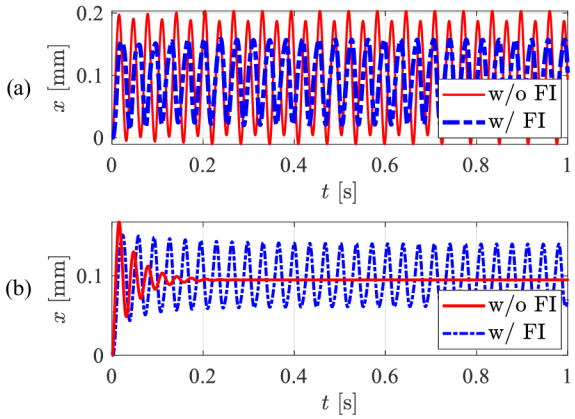

FIGURE 5: SIMULATED TABLE POSITION OF THE STAGE W/ AND W/O FI USING $\dot{x}_p = 20$ mm/s, $k = 6 \times 10^4$ N/m AND (A) $c = 10$ Ns/m; (B) $c = 100$ Ns/m.

Fig. 5 compares the response of the PD-controlled stage with and without FI, when the platform is moving at a constant velocity of $\dot{x}_p = 20$ mm/s. When c is relatively small, both stages with and without FI suffer from stick-slip oscillations at steady-state, but the stage with FI exhibits smaller oscillation amplitude than that without FI. This may be due to the isolation effects of FI, as it low-pass filters part of the oscillation that is injected to the system through bearing motion. As c increases to 100 Ns/m, the friction-induced vibration of the stage without FI is effectively attenuated. This is expected since an increase in the overall damping of the system is well-known to be able to mitigate stick-slip vibration [14]. However, the stage with FI still suffers from persistent oscillations even with a relatively large value of c.

Fig. 6 compares the stability charts of the PD-controlled stage with and without FI when the platform is moving at different constant velocities. Stability here is defined as the absence of persistent friction-induced oscillations during the motion. Observe that the stability characteristics of the system without FI is very predictable; regardless of the platform velocity, friction-induced instability can be mitigated by increasing the servo controller gains, especially the damping c. With the addition of the FI, stabilizing the motion stage becomes less straightforward, and the range of servo parameters that

stabilize the stage becomes smaller than the corresponding case without FI.

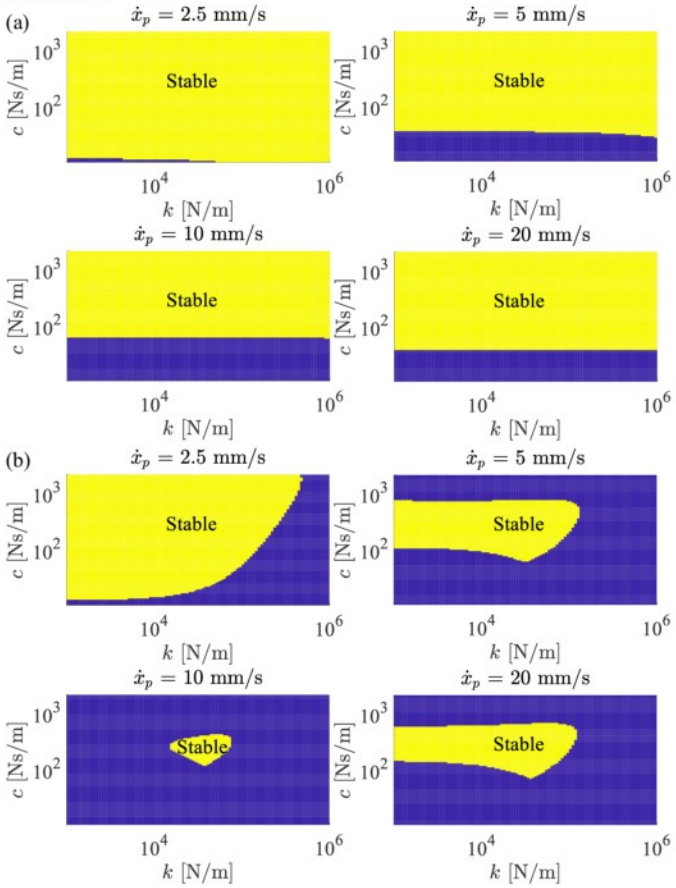

FIGURE 6: STABILITY CHARTS OF THE STAGE (A) W/O AND (B) W/ FI.

4.3. Linear Stability Analysis

The stability charts in Fig. 6 above are generated by numerically simulating the responses of the stage using zero initial condition (i.e., $x = x_b = \dot{x} = \dot{x}_b = 0$); there is no guarantee that the system will remain stable under other initial conditions. Therefore, linear stability analysis is carried out to obtain a general understanding of the system stability in the vicinity of equilibrium points. The state equations can be written in non-dimensional form by defining natural frequency ω_n and dimensionless time τ as

$$\omega_n = \sqrt{\frac{k}{m_t + m_b}}\ ;\ \tau = \omega_n t \tag{11}$$

This leads to the following dimensionless variables

$$\begin{aligned} &X = \frac{x}{L};\ X_p = \frac{x_p}{L};\ \dot{X} = \frac{dX}{d\tau} = \frac{\dot{x}}{\omega_n L};\ Z = \frac{z}{L}; \\ &V = \frac{dX - dX_p}{d\tau} = \frac{\dot{x} - \dot{x}_p}{\omega_n L};\ \dot{V} = \frac{\ddot{x}}{\omega_n^2 L};\ \dot{Z} = \frac{dZ}{d\tau} = \frac{\dot{z}}{\omega_n L} \end{aligned} \tag{12}$$

and dimensionless parameters

$$\zeta = \frac{c}{2m_t\omega_n};\ \kappa_2 = \frac{\sigma_0}{k};\ \eta_2 = \frac{\sigma_2}{c};\ \gamma_2 = \frac{\sigma_1}{c}; \tag{13}$$

$$V_s = \frac{v_s}{\omega_n L};\ F_C = \frac{f_C}{kL};\ F_S = \frac{f_S}{kL};\ H(V) = \frac{|V|}{G(V)};$$

$$\kappa_2 G(V) = F_C + (F_S - F_C)e^{-(V/V_s)^2}$$

where L is an arbitrary length. Substituting Eqs. (11)-(13) into (8), the dimensionless state equations of the PD-controlled motion stage without FI are given by

$$\begin{aligned} &\Delta_1 = \begin{bmatrix} X & V & Z \end{bmatrix}^T; \\ &\dot{\Delta}_1 = \begin{bmatrix} V + \dot{X}_p & -(F_i + F_f) & V - H(V)Z \end{bmatrix}^T \end{aligned} \tag{14}$$

where

$$\begin{aligned} F_i &= 2\zeta\dot{X} + X = 2\zeta\left(V + \dot{X}_p\right) + X \\ F_f &= \left(\kappa_2 - 2\zeta\gamma_2 H(V)\right)Z + 2\zeta\left(\gamma_2 + \eta_2\right)V \end{aligned} \tag{15}$$

The equilibriums can then be derived as

$$\begin{aligned} \Delta_{1,1} &= \begin{bmatrix} \int V\,d\tau + X_p + C_X \\ 0 \\ -\dfrac{\left(\int V\,d\tau + X_p + C_X + 2\zeta\dot{X}_p\right)}{\kappa_2} \end{bmatrix}; \\ \Delta_{1,2} &= \begin{bmatrix} -\kappa_2 \mathrm{sgn}\left(-\dot{X}_p\right)G\left(-\dot{X}_p\right) + 2\zeta\eta_2\dot{X}_p \\ -\dot{X}_p \\ \mathrm{sgn}\left(-\dot{X}_p\right)G\left(-\dot{X}_p\right) \end{bmatrix} \end{aligned} \tag{16}$$

where C_X is the initial displacement of the table, $\Delta_{1,1}$ represents the sticking equilibrium (i.e., $v = 0$) and $\Delta_{1,2}$ represents the slipping equilibrium (i.e., $z = \mathrm{sgn}(v)\mathrm{g}(v)$). Note that $\Delta_{1,1}$ and $\Delta_{1,2}$ overlap when $\dot{x}_p = 0$, as discussed in Section 4.1. The Jacobian matrices at these equilibriums are denoted as $J_{1,1}$ and $J_{1,2}$

$$\begin{aligned} J_{1,1} &= \begin{bmatrix} 0 & 1 & 0 \\ -1 & -2\zeta - 2\zeta\eta_2 - 2\zeta\gamma_2 & -\kappa_2 \\ 0 & 1 & 0 \end{bmatrix}; \\ J_{1,2} &= \begin{bmatrix} 0 & 1 & 0 \\ -1 & -2\zeta A_1 & -\kappa_2 + 2\zeta\gamma_2 H\left(\dot{X}_p\right) \\ 0 & \Gamma(\dot{X}_p) & -H\left(\dot{X}_p\right) \end{bmatrix} \end{aligned} \tag{17}$$

where

$$\begin{aligned} G'(V) &= \frac{\partial G}{\partial V} = -(F_S - F_C)e^{-\left(\frac{V}{V_s}\right)^2}\left(\frac{2V}{\kappa_2 V_s^2}\right); \\ \Gamma(\dot{X}_p) &= \frac{\dot{X}_p G'\left(\dot{X}_p\right)}{G\left(\dot{X}_p\right)};\ A_1 = \left(1 + \eta_2 + \gamma_2\Gamma(\dot{X}_p)\right) \end{aligned} \tag{18}$$

Observe that $J_{1,1}$ is independent of $\dot{x}_p$, and $J_{1,2}$ is unaffected by the direction of $\dot{x}_p$. Focusing on the stability of the slipping equilibrium ($\Delta_{1,2}$), we can obtain the characteristic equation as

$$\left|\lambda I_3 - J_{1,2}\right| = 0 \Rightarrow a_0\lambda^3 + a_1\lambda^2 + a_2\lambda + a_3 = 0 \tag{19}$$

where

$$\begin{aligned} &a_0 = 1; a_1 = 2\zeta + H\left(\dot{X}_p\right) + 2\eta_2\zeta + 2\gamma_2\zeta\Gamma\left(\dot{X}_p\right); \\ &a_2 = \kappa_2\Gamma\left(\dot{X}_p\right) + 2\zeta H\left(\dot{X}_p\right) + 2\eta_2\zeta H\left(\dot{X}_p\right) + 1; a_3 = H\left(\dot{X}_p\right) \end{aligned} \tag{20}$$

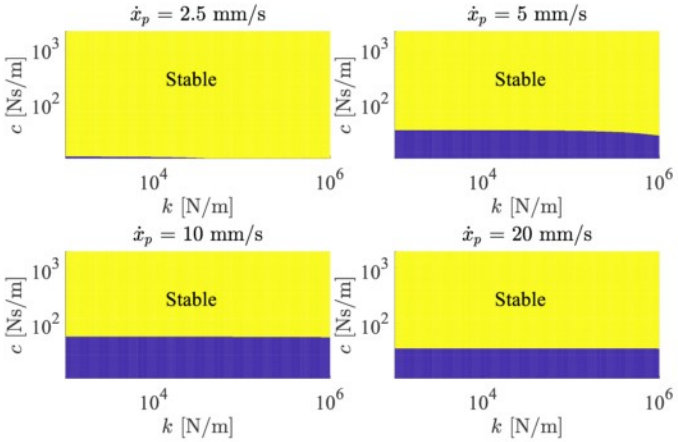

FIGURE 7: STABILITY CHARTS OF THE PD-CONTROLLED STAGE WITHOUT FI AT SLIPPING EQUILIBRIUM (I.E., $\Delta_{1,2}$).

Using Routh-Hurwitz criterion [19], it can be shown that the system is stable if $a_0a_1 > 0$ and $(a_1a_2 - a_0a_3)/a_2 > 0$. Fig. 7 shows the linear stability charts of the PD-controlled stage without FI using different parameters of k and c. Note that measured parameters from the stage of Fig. 3 are used – see Table 1. Although the region of stability varies for different platform velocities $\dot{x}_p$, it is quite adequate for a wide range of k and c combinations. In particular, the equilibrium is stable if k and c are large enough.

Similarly, the state equations of the PD-controlled stage with FI can be written in dimensionless form using

$$X_b = \frac{x_b}{L};\ \dot{X}_b = \frac{dX_b}{d\tau} = \frac{\dot{x}_b}{\omega_n L};\ \kappa_1 = \frac{k_j}{k};\ \eta_1 = \frac{c_j}{c};$$
$$\rho = \frac{m_b}{m_t};\ \omega_n = \sqrt{\frac{k}{m_t}};\ V = \frac{\dot{x}_b - \dot{x}_p}{\omega_n L};\ \dot{V} = \frac{d^2X_b}{d\tau^2} = \frac{\ddot{x}_b}{\omega_n^2 L} \tag{21}$$

together with the previously defined dimensionless parameters (see Eqs. (11)-(13)). The non-dimensional state equations are then given by

$$\Delta_2 = \begin{bmatrix} X & \dot{X} & X_b & V & Z \end{bmatrix}^T;$$
$$\dot{\Delta}_2 = \begin{bmatrix} \dot{X} & -(F_i + F_l) & V + \dot{X}_p & -\dfrac{F_f - F_l}{\rho} & V - H(V)Z \end{bmatrix}^T \tag{22}$$

where

$$F_l = 2\zeta\eta_1\left(\dot{X} - V - \dot{X}_p\right) + \kappa_1\left(X - X_b\right) \tag{23}$$

The sticking equilibrium $\Delta_{2,1}$ and slipping equilibrium $\Delta_{2,2}$ of the system are obtained as

$$\Delta_{2,1} = \begin{bmatrix} \dfrac{-2\zeta\dot{X}_p + \kappa_1 D_b}{1+\kappa_1} \\ \dot{X}_p \\ D_b \\ 0 \\ -\dfrac{\kappa_1(1+\kappa_1)D_b + \left(2\zeta\dot{X}_p - \kappa_1 D_b\right)}{\kappa_2(1+\kappa_1)} \end{bmatrix}; \tag{24}$$

$$\Delta_{2,2} = \begin{bmatrix} -\kappa_2 B_1\left(-\dot{X}_p\right) - 2\zeta\eta_2\dot{X}_p \\ 0 \\ -\dfrac{(1+\kappa_1)\left(-\kappa_2 B_1\left(-\dot{X}_p\right) - 2\zeta\eta_2\dot{X}_p\right)}{\kappa_1} \\ -\dot{X}_p \\ B_1\left(-\dot{X}_p\right) \end{bmatrix}$$

where

$$D_b = \int V\, d\tau + X_p + C_b;$$
$$B_1\left(\dot{X}_p\right) = \mathrm{sgn}\left(\dot{X}_p\right) G\left(\dot{X}_p\right) \tag{25}$$

and C_b is the initial displacement of m_b. The Jacobian matrices of these two equilibriums are obtained as

$$J_{2,1} = \begin{bmatrix} 0 & 1 & 0 & 0 & 0 \\ -\kappa_1 - 1 & -2\zeta(\eta_1 + 1) & \kappa_1 & 2\zeta\eta_1 & 0 \\ 0 & 0 & 0 & 1 & 0 \\ \dfrac{\kappa_1}{\rho} & \dfrac{2\zeta\eta_1}{\rho} & -\dfrac{\kappa_1}{\rho} & -\dfrac{2\zeta A_2}{\rho} & -\dfrac{\kappa_2}{\rho} \\ 0 & 0 & 0 & 1 & 0 \end{bmatrix};$$
$$J_{2,2} = \begin{bmatrix} 0 & 1 & 0 & 0 & 0 \\ -\kappa_1 - 1 & -2\zeta(\eta_1 + 1) & \kappa_1 & 2\zeta\eta_1 & 0 \\ 0 & 0 & 0 & 1 & 0 \\ \dfrac{\kappa_1}{\rho} & \dfrac{2\zeta\eta_1}{\rho} & -\dfrac{\kappa_1}{\rho} & -\dfrac{2\zeta A_3}{\rho} & -\dfrac{A_4}{\rho} \\ 0 & 0 & 0 & \Gamma\left(\dot{X}_p\right) & -H\left(\dot{X}_p\right) \end{bmatrix} \tag{26}$$

where

$$A_2 = \eta_1 + \eta_2 + \gamma_2;\ A_3 = \left(\eta_1 + \eta_2 + \gamma_2\Gamma\left(\dot{X}_p\right)\right);$$
$$A_4 = \kappa_2 - 2\zeta\gamma_2 H\left(\dot{X}_p\right) \tag{27}$$

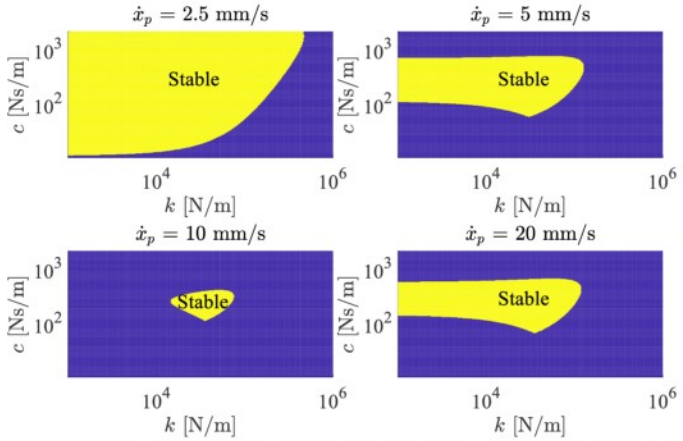

FIGURE 8: STABILITY CHARTS OF THE PD-CONTROLLED STAGE WITH FI AT SLIPPING EQUILIBRIUM (I.E., $\Delta_{2,2}$).

Again, it can be observed that $J_{2,1}$ is independent of $\dot{x}_p$, and $J_{2,2}$ is unaffected by the direction of $\dot{x}_p$. The closed-form expressions of Routh-Hurwitz for the case of the stage with FI are not presented here for brevity. They are evaluated using Matlab and the obtained stability charts in the vicinity of $\Delta_{2,2}$ are shown in Fig. 8 using different k and c values. The stability of

the PD-controlled stage with FI is jeopardized when large values of c and k are employed. This finding agrees with the numerical stability analysis, indicating that the linear analysis about the slipping equilibrium is reliable.

Fig. 9 depicts the influence of some design parameters on the stability of the stage with FI. These parameters include – the stiffness parameter κ_1, damping parameter η_1 and mass ratio ρ. The coefficient α and β are multipliers for the redefinition of $\kappa_1 = \alpha\kappa_1$, $\eta_1 = \alpha\eta_1$ and $\rho = \beta\rho$ used for the stability region analysis. As shown in Fig. 10, the stability of the system improves as α increases. A large α, however, can diminish the effect of the FI since the link between the two bodies becomes more rigid, thus potentially affecting the isolation performance. Increasing β, particularly to $\beta \approx 0.5$, improves the stability of the system. These observations can be crucial for the design optimization of the system for balancing stability and performance criteria.

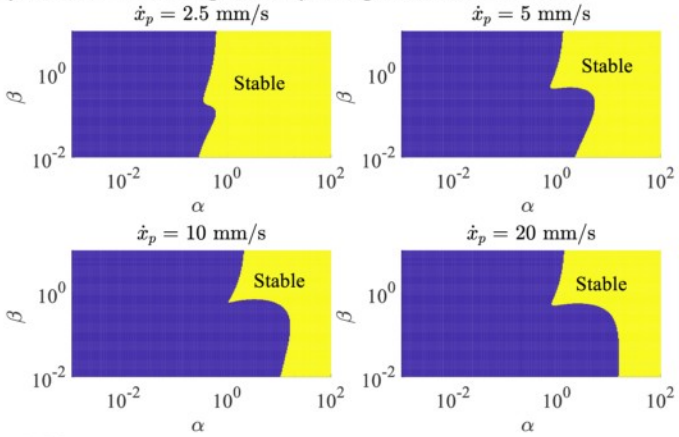

FIGURE 9: STABILITY CHARTS OF THE STAGE WITH FI AT SLIPPING EQUILIBRIUM WITH RESPECT TO α AND β ($k = 1 \times 10^5$ N/m AND $c = 250$ Ns/m).

5. DISCUSSION

5.1. Nonlinear Stability Analysis

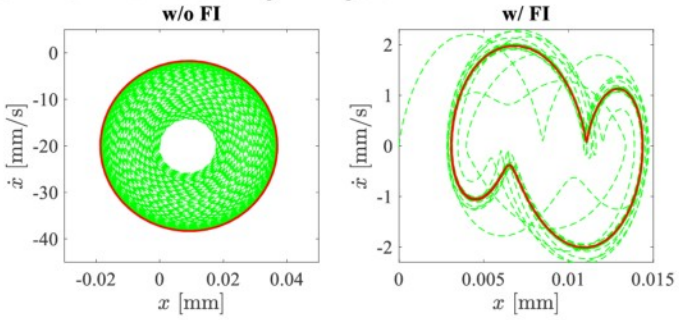

FIGURE 10: PHASE PORTRAITS OF THE STAGE WITH AND WITHOUT FI USING $k = 6.5 \times 10^5$ N/m, $c = 250$ Ns/m AND $\dot{x}_p = 20$ mm/s (DASH: PHASE TRAJECTORIES; SOLID: LIMIT CYCLES).

In the presence of LuGre friction, analytical models of the PD-controlled stage with and without FI are highly nonlinear, which leads to some interesting observations. For example, as shown in Fig. 10, while the systems are not able to converge to the fixed points, the phase trajectories of x and v show convergences at stable limit cycles. Figure 10 also shows the beneficial effect of FI, as the system with FI exhibits approximately a tenfold smaller limit cycle amplitude. While the presence of FI decreases the linear stability region of the system, the nonlinear analysis shows that the effect of the friction-induced vibration is reduced significantly by the FI. This is especially beneficial to positioning performance in practice where model uncertainties exist.

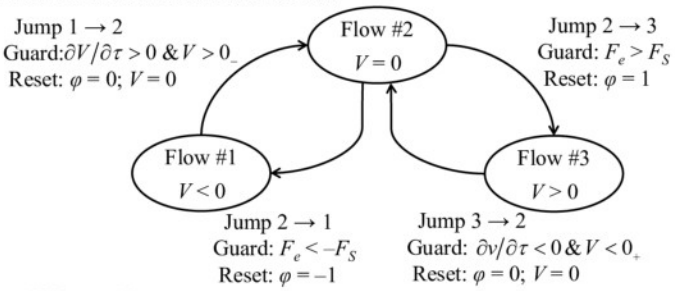

FIGURE 11: THE HYBRID DYNAMIC FLOWCHART OF THE STICK-SLIP MODELS.

Moreover, the LuGre friction dynamics is non-smooth due to the existence of sgn(V) and $|V|$, since the derivatives of both terms with respect to V do not exist at $V = 0$. The depiction of the dynamic flows and jumps of the stick-slip models as hybrid systems is shown in Fig. 11. Here, for the system without FI, $F_e = -F_i$. For the system with FI, $F_e = -F_l$. The state φ is introduced to replace the non-smooth term sgn(V) such that $|V| = \varphi V$. The discrete jumps between the flows occur when the guard conditions are triggered, while the reset functions assign new values to the states whenever the jumps occur.

It is not guaranteed that the stability at each smooth dynamic flow will lead to a stable hybrid system. Therefore, the servo controller is required to fulfill certain sufficient nonlinear stability conditions, such as the stability of a common Lyapunov function or multiple Lyapunov functions [20][21]. Our future work will include a thorough nonlinear and hybrid dynamical system analysis, which will be crucial to the improvement of FI and servo controller design.

5.2. Effects of Servo Force (f_{servo})

In Section 4.2 simulation analysis is carried out on the PD-controlled motion stage (i.e., $f_{servo} = 0$) with and without FI. However, this neglects another important servo force – integral action. Integral controller is widely used in precision motion stages to suppress the steady-state error caused by disturbances in the system, e.g., friction force [1]. Fig. 12 (a) shows the response of the motion stage with FI using different gains for the integral controller (i.e., k_i). Based on the stability chart obtained in Fig. 6 (b), a set of servo gains is selected to stabilize the system (i.e., $k = 2 \times 10^4$ N/m and $c = 100$ Ns/m). Although the table is free from friction-induced oscillation, it stays at 0.3 mm during steady-state. With the addition of an integral action ($k_i = 1 \times 10^5$ N/(m·s)), the servo controller is able to bring the table back to the desired zero location (i.e., $x = 0$ mm). In general, a larger integral gain is desired to quickly reject the disturbance force. However, the stage starts suffering from severe oscillation at steady-state when an integral gain of 1×10^6 N/(m·s) is used. As shown from the phase trajectories in Fig 12 (b), further

increasing it to 5 × 10^6 N/(m·s) leads to chaotic oscillatory behavior, making the system response very sensitive to the initial conditions. To facilitate the controller design, it is necessary to investigate the effects of f_{servo} on the response and stability of the servo-controlled stage with FI. Any other servo force that is commonly used in precision applications (e.g., feedforward action and DOB) can also be applied in future studies.

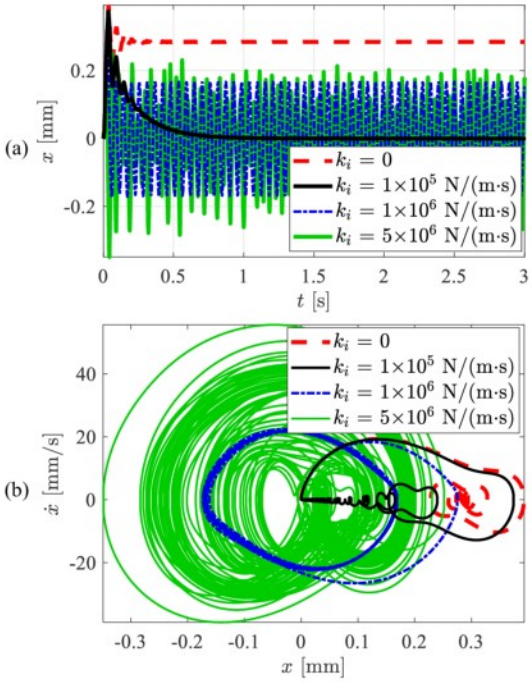

FIGURE 12: (A) SIMULATED TABLE POSITION OF THE STAGE WITH FI AND (B) PHASE PORTRAIT USING $\dot{x}_p = 20$ mm/s, $k = 2 \times 10^4$ N/m AND $c = 100$ Ns/m.

5.3. Effects of External Excitation

In tracking applications, the motion stage is often commanded to follow a desired trajectory such as the circle tests shown in Section 2.2. In this case, the moving table of the stage (i.e., m_t) in Fig. 4 (a) is no longer connected to the ground but connected to a reference command (i.e., x_r) instead. Accordingly, the dynamics of the PD-controlled stage with FI is given by

$$\begin{aligned} &m_t\ddot{x} + c(\dot{x} - \dot{x}_r) + k(x - x_r) + c_j(\dot{x} - \dot{x}_b) + k_j(x - x_b) = 0; \\ &m_b\ddot{x}_b + f_f + c_j(\dot{x}_b - \dot{x}) + k_j(x_b - x) = 0 \end{aligned} \tag{28}$$

Fig. 13 shows the simulated system response when a sinusoidal command is used as the reference trajectory, i.e., $x_r = \sin(0.2\pi t))$ mm. When the moving platform is stationary (i.e., $\dot{x}_p = 0$), it is observed that the bearing motion (i.e., x_b) suffers from severe stiction at each velocity reversal of the sinusoidal motion. Due to the isolation effects of FI, the table position (i.e., x) can roughly follow the reference command without stiction. However, it is observed that x still suffers from non-smooth behavior as the friction transitions from pre-motion to gross motion regime at velocity reversals. Interestingly, when the platform is moving at a small speed (i.e., $\dot{x}_p$ = 1 mm/s), the undesirable effect of stiction on the table and bearing motion is effectively mitigated. To understand the effects of x_r and its interaction with $\dot{x}_p$, stability and bifurcation analysis of the stage with FI in the presence of external excitation (i.e., $x_r \neq 0$) and self-excitation (i.e., $\dot{x}_p \neq 0$) will be carried out in the future.

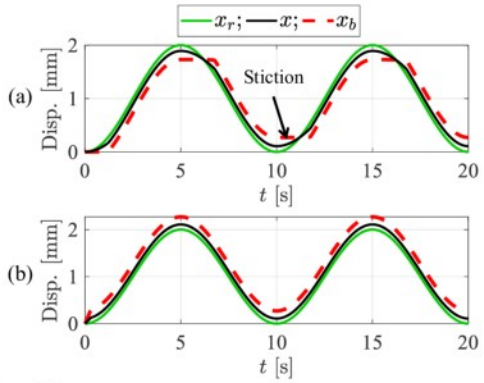

FIGURE 13: SIMULATED RESPONSE OF THE PD-CONTROLLED STAGE WITH FI USING $k = 6 \times 10^4$ N/m, $c = 100$ Ns/m, $x_r = \sin(0.2\pi t)$ mm AND (A) $\dot{x}_p = 0$ mm/s; (B) $\dot{x}_p = 1$ mm/s.

5.4. Mode Coupling

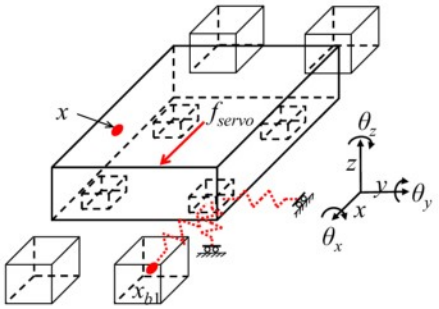

FIGURE 14: SCHEMATIC OF A HIGH ORDER MODEL OF THE PRECISION MOTION STAGE WITH FOUR FIS.

In the previous analysis, a simplified model of the servo-controlled motion stage with FI is utilized. The stage is modeled as a table of mass m_t and a bearing of mass m_b, both have only one DOF in the motion direction; note that m_b accounts for the combined mass of bearing and FI. In practice, two or four mechanical bearings are often implemented on the stage which may lead to mode coupling instability. As shown in Fig. 14, a high order model of the precision motion stage with four bearings (and FIs) is proposed to study the effects of mode coupling. The moving table of the stage is modeled as a rigid body with 6-DOF (i.e., 3 translational and 3 rotational) and each bearing is modeled as a simple mass with 1-DOF in the motion direction. In the case where friction dynamics and/or FI parameters of each bearing are different, potentially harmful phenomena may be observed because of mode coupling.

6. CONCLUSIONS AND FUTURE WORK

This introductory paper has examined the influence of friction isolator on the performance and stability of a precision motion stage. The friction isolator is a machine element that is very compliant in the motion direction of a servo-controlled stage. It is placed between the mechanical bearings and moving table of a motion stage, thus effectively isolating the stage from deleterious effects of friction. It was experimentally shown that

the undesirable effects of pre-motion friction on the accuracy and speed of precision motion stage can be effectively mitigated using a friction isolator. With the addition of friction isolator, the very stiff and variable pre-motion frictional stiffness is replaced with a much softer and less variable stiffness, making it easier for the model-based friction compensators to deliver high performance and superior robustness. However, numerical studies on a rudimentary dynamic model of a PD-controlled motion stage with LuGre friction showed that the addition of friction isolator shrinks the range of servo gains that can stabilize the motion stage. Linear stability analysis in the vicinity of equilibriums confirmed the numerical results.

Future work will focus on nonlinear stability analysis of the servo-controlled stage with friction isolator by implementing a hybrid dynamic model of LuGre friction. This will, for instance, provide general knowledge about the de-stabilizing effects of friction isolator and facilitate controller designs with guaranteed global stability. Moreover, the effects of mode coupling will be investigated using a high order model of the motion stage with multiple friction isolators. On the practical side, future work will include other commonly used servo controllers (e.g., integral controller) and external excitation to obtain a deeper and generalizable understanding of the influence of friction isolator on the design and control of precision motion stage.

ACKNOWLEDGEMENTS

This work is funded by National Science Foundation (NSF) Award CMMI #1562297: Vibration Assisted Nanopositioning: An Enabler of Low-cost, High- throughput Nanotech Processes and CMMI #1855390: Towards a Fundamental Understanding of a Simple, Effective and Robust Approach for Mitigating Friction in Nanopositioning Stages

APPENDIX

The parameters of LuGre model shown in Table 1 is identified on the precision motion stage; note that the friction isolators are deactivated by installing the fixtures. When friction is in the gross motion regime, the rate of bristle deflection is zero (i.e., $\dot{z} = 0$), that is

$$z_{ss} = g(v)\mathrm{sgn}(v) \tag{29}$$

Substituting Eqs. (5) and (29) into (6), the steady-state friction force during gross motion is given by [18]

$$f_{f,ss} = \left[f_c + (f_s - f_c)e^{-(v/v_s)^2} \right] \mathrm{sgn}(v) + \sigma_2 v \tag{30}$$

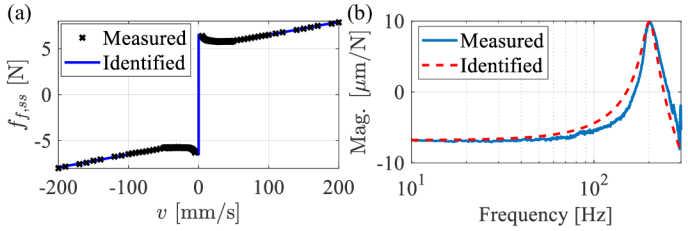

FIGURE 15: MEASURED AND IDENTIFIED (A) $f_{f,ss}$ VS v CURVE AND (B) MAGNITUDE PLOTS OF FREQUENCY RESPONSE FUNCTION (FRF) FROM SERVO FORCE TO TABLE DISPLACEMENT.

The steady-state friction force $f_{f,ss}$ is obtained by commanding the stage to travel at different levels of constant velocity (CV) and measuring the servo force required to maintain the CV motion. Fig. 15 (a) shows the measured $f_{f,ss}$ versus v curve. The related parameters (i.e., f_C, f_S, v_s and σ_2) are identified by using nonlinear least squares to fit the measured data.

The remaining parameters are identified using a simple model of an open-loop controlled stage with LuGre friction

$$(m_t + m_b)\ddot{x} = -\left[\sigma_0 z + \sigma_1 \left(\dot{x} - \frac{|\dot{x}|}{g(\dot{x})} z \right) + \sigma_2 \dot{x} \right] + f_{servo} \tag{31}$$

Linearizing the above equation for the pre-motion friction regime (i.e., at equilibrium $x = z = 0$), yields [22]

$$(m_t + m_b)\ddot{x} = -\left[\sigma_0 x + (\sigma_1 + \sigma_2)\dot{x} \right] + f_{servo} \tag{32}$$

Using Laplace transformation, the frequency response function (FRF) from servo force to table displacement is obtained as

$$G(s) = \frac{1}{(m_t + m_b)s^2 + (\sigma_1 + \sigma_2)s + \sigma_0} \tag{33}$$

The measured FRF (i.e., G) is obtained by applying a constant-amplitude sinusoidal force input commands with varying frequencies to the servo motor and recording the corresponding output displacement magnitudes of the table's position using the linear encoder. The parameters (i.e., σ_0 and σ_1) are obtained through least-square-fitting of the measured FRF with $m_t + m_b = 1.5$ kg. Fig. 15 (b) shows an excellent fit between the measured and identified FRFs.

REFERENCES

[1] Altintas, Y., Verl, A., Brecher, C., Uriarte, L., and Pritschow, G., 2011, "Machine tool feed drives," *Annals of the CIRP*, ***60***(2), pp.779-796.

[2] Al-Bender, F., and Swevers, J., 2008, "Characterization of friction force dynamics," *IEEE Control Systems Magazine*, ***28***(6), pp.64-81.

[3] Marques, F., Flores, P., Claro, J.P., and Lankarani, H.M., 2016, "A survey and comparison of several friction force models for dynamic analysis of multibody mechanical systems," *Nonlinear Dynamics*, ***86***(3), pp.1407-1443.

[4] Futami, S., Furutani, A., and Yoshida, S., 1990, "Nanometer positioning and its micro-dynamics," *Nanotechnology*, ***1***(1), pp.31.

[5] Armstrong-Hélouvry, B., Dupont, P., and De Wit, C.C., 1994, "A survey of models, analysis tools and compensation methods for the control of machines with friction," *Automatica*, ***30***(7), pp.1083-1138.

[6] Hensen, R.H., Van de Molengraft, M.J.G., and Steinbuch, M., 2003, "Friction induced hunting limit cycles: a comparison between the LuGre and switch friction model," *Automatica*, ***39***(12), pp.2131-2137.

[7] Maeda, Y., and Iwasaki, M., 2013, "Rolling friction model-based analyses and compensation for slow settling response in precise positioning," *IEEE Transactions on Industrial Electronics*, ***60***(12), pp.5841-5853.

[8] Dong, X., Yoon, D., and Okwudire, C.E., 2017, "A novel approach for mitigating the effects of pre-rolling/pre-sliding friction on the settling time of rolling bearing nanopositioning stages using high frequency vibration," *Precision Engineering*, ***47***, pp.375-388.

[9] Dong, X., Liu, X., Yoon, D., and Okwudire, C.E., 2017, "Simple and robust feedforward compensation of quadrant glitches using a compliant joint," *Annals of the CIRP*, ***66***(1), pp.353-356.
[10] Dong, X., and Okwudire, C.E., 2018, "An experimental investigation of the effects of the compliant joint method on feedback compensation of pre-sliding/pre-rolling friction," *Precision Engineering*, ***54***, pp.81-90.
[11] Mokha, A., Constantinou, M.C., Reinhorn, A.M., and Zayas, V.A., 1991, "Experimental study of friction-pendulum isolation system," *Journal of Structural Engineering*, ***117***(4), pp.1201-1217.
[12] Dong, X., and Okwudire, C.E., 2017, "Detailed experimental evaluation of the compliant Joint method for feedforward compensation of pre-motion friction," *32th ASPE Annual Meeting*, ***67***, pp.52-56.
[13] Oestreich, M., Hinrichs, N., and Popp, K., 1996, "Bifurcation and stability analysis for a non-smooth friction oscillator," *Archive of Applied Mechanics*, ***66***(5), pp.301-314.
[14] Hinrichs, N., Oestreich, M., and Popp, K., 1998, "On the modelling of friction oscillators," *Journal of sound and Vibration*, ***216***(3), pp.435-459.
[15] Hoffmann, N.P., 2007, "Linear stability of steady sliding in point contacts with velocity dependent and LuGre type friction," *Journal of Sound and Vibration*, ***301***(3-5), pp.1023-1034.
[16] Van de Vrande, B.L., Van Campen, D.H., and De Kraker, A., 1999, "An approximate analysis of dry-friction-induced stick-slip vibrations by a smoothing procedure," *Nonlinear Dynamics*, ***19***(2), pp.159-171.
[17] Nakano, K., and Maegawa, S., 2009, "Stick-slip in sliding systems with tangential contact compliance," *Tribology International*, ***42***(11-12), pp.1771-1780.
[18] De Wit, C.C., Olsson, H., Astrom, K.J., and Lischinsky, P., 1995, "A new model for control of systems with friction," *IEEE Transactions on Automatic Control,* ***40***(3), pp.419-425.
[19] Ogata, K., and Yang, Y., 2002, "Modern control engineering," *Prentice-Hall*.
[20] Márton, L., and Lantos, B., 2009, "Control of mechanical systems with Stribeck friction and backlash," *Systems & Control Letters* ***58***(2), pp.141-147.
[21] Branicky, M.S., 1998, "Multiple Lyapunov functions and other analysis tools for switched and hybrid systems," *IEEE Transactions on Automatic Control*, ***43***(4), pp.475-482.
[22] Hensen, R.H., van de Molengraft, M.J., and Steinbuch, M., 2002, "Frequency domain identification of dynamic friction model parameters," *IEEE Transactions on Control Systems Technology*, ***10***(2), pp.191-196.